



Nonequilibrium and nonlinear dynamics in Berea and Fontainebleau sandstones: Low-strain regime

Donatella Pasqualini,¹ Katrin Heitmann,² James A. TenCate,³ Salman Habib,⁴ David Higdon,⁵ and Paul A. Johnson³

Received 8 January 2006; revised 20 June 2006; accepted 11 September 2006; published 23 January 2007.

[1] Members of a wide class of geomaterials are known to display complex and fascinating nonlinear and nonequilibrium dynamical behaviors over a wide range of bulk strains, down to surprisingly low values, e.g., 10^{-7} . In this paper we investigate two sandstones, Berea and Fontainebleau, and characterize their behavior under the influence of very small external forces via carefully controlled resonant bar experiments. By reducing environmental effects due to temperature and humidity variations, we are able to systematically and reproducibly study dynamical behavior at strains as low as 10^{-9} . Our study establishes the existence of two strain regimes separated by ϵ_M . At strains below ϵ_M the material is nonlinear and quasi-equilibrium thermodynamics applies as evidenced by the success of Landau theory and a simple macroscopic description based on the Duffing oscillator. At strains above ϵ_M the behavior becomes truly nonequilibrium, as demonstrated by the existence of material conditioning, and Landau theory no longer applies. The main focus of this paper is the study of the first region, but we also comment on how our work clarifies and resolves previous experimental conflicts, as well as suggest new directions of research.

Citation: Pasqualini, D., K. Heitmann, J. A. TenCate, S. Habib, D. Higdon, and P. A. Johnson (2007), Nonequilibrium and nonlinear dynamics in Berea and Fontainebleau sandstones: Low-strain regime, *J. Geophys. Res.*, 112, B01204, doi:10.1029/2006JB004264.

1. Introduction

[2] Geomaterials display very interesting nonlinear features, diverse aspects of which have been investigated over a long period of time. For a recent overview see, e.g., *Ostrovsky and Johnson* [2001, and references therein]. A standard technique used to study these nonlinear features is the resonant bar experiment [*Clark*, 1966; *Jaeger and Cook*, 1979; *Carmichael*, 1984; *Bourbie et al.*, 1987]. In these experiments a long rod of the material under test is driven longitudinally and its amplitude and frequency response monitored. For a linear material the resonance frequency of the rod is invariant over a very wide range of dynamical strain. An example of this behavior is shown in the results from one of our experiments on acrylic in Figure 1a: increasing the strain up to 2×10^{-6} leaves the resonance frequency unchanged (note that the x axis shows the change

in the resonance frequency, Δf , and not the resonance frequency itself). The resonance frequency of a rod made from a nonlinear material such as Berea sandstone behaves quite differently: When a driving force is applied to the rod, the frequency either increases or decreases (the modulus either hardens or softens) depending on the precise properties of the material. This phenomenon is well known, and a theoretical description based on quasi-equilibrium thermodynamics and nonlinear elasticity has existed for a long time [see, e.g., *Landau and Lifshitz*, 1998]; we will refer to this as the classical theory of nonlinear elasticity or simply as Landau theory.

[3] Many geomaterials, such as sandstones, belong to the general class of nonlinear materials. Figures 1b and 1c display resonant bar results for two representative samples, Berea and Fontainebleau. In both cases the shift in resonance frequency is very large and the resonance frequency decreases with drive amplitude. The strength of the nonlinear response in these materials is very large, orders of magnitude more than for metals. Consequently, it is important to check whether Landau theory still applies to these materials, and, if so, over what range of strains.

[4] It is widely believed that geomaterials behave differently than weakly nonlinear materials because of their complex internal structure. They are formed by an assembly of more or less rigid “grains” connected via a much softer “bond” network of varying porosity. The grains make up a large fraction of the volume, between 80 and 99%. Individual grains can be very pure (as in the case of Fontainebleau, $\sim 99 +$ % quartz) or made up from several different

¹Environmental Geology and Spatial Analysis Group, Earth and Environmental Sciences Division, University of California, Los Alamos National Laboratory, Los Alamos, New Mexico, USA.

²Space and Atmospheric Sciences Group, University of California, Los Alamos National Laboratory, Los Alamos, New Mexico, USA.

³Geophysics Group, Earth and Environmental Sciences Division, University of California, Los Alamos National Laboratory, Los Alamos, New Mexico, USA.

⁴Elementary Particles and Field Theory, University of California, Los Alamos National Laboratory, Los Alamos, New Mexico, USA.

⁵Statistical Sciences Group, University of California, Los Alamos National Laboratory, Los Alamos, New Mexico, USA.

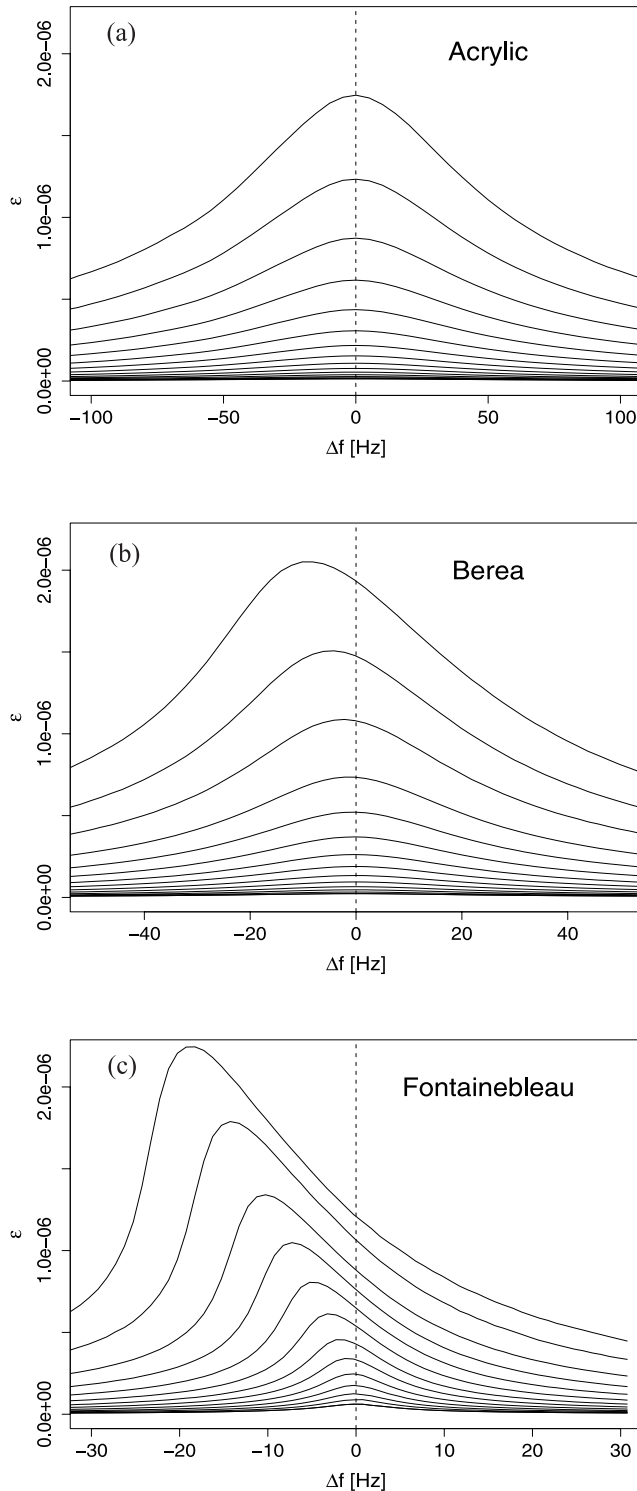


Figure 1. Resonance curves for (a) acrylic, (b) Berea, and (c) Fontainebleau at different drives. Acrylic is a linear material used as a control in the experiments. Nonlinearity is evidenced in Berea and Fontainebleau samples by the shift in the peak of the resonance curves. The reference center frequency is 2150 Hz for acrylic, 2765 Hz for Berea, and 1155.98 Hz for Fontainebleau.

components (as in the case of Berea: 85% quartz, 8% feldspar, plus small quantities of other minerals). Most of these materials are quite porous and their behavior changes dramatically under the influence of environmental effects, such as temperature [see, e.g., *Sheriff*, 1973] or humidity [see, e.g., *Gordon and Davis*, 1968; *O'Hara*, 1985; *Zinszner et al.*, 1997; *Van den Abeele et al.*, 2002]. This sensitivity to the environment makes controlled studies difficult, as the experiments must be carried out in such a way that these effects are demonstrably under control.

[5] Another difficulty in measuring the frequency response of sandstones arises from the brittleness of rocks. If the samples are driven too hard, microcracks can be induced and the resulting behavior of the material can change dramatically. In addition, driving can also induce long-lived nonequilibrium macrostates that relax back over a long period of time (approximately hours). Thus it is important to ensure, by repeating a given drive protocol on the same sample and verifying that the material response does not change from one experiment to the next, that the samples have not been altered from their original condition and the environment is unchanged over the set of observations. The experiments described in this paper were carried out in this way. Furthermore, the very low strain values ensured that sample damage rarely occurred.

[6] One goal of this work is to clarify, using new and existing data, conflicting observations in the literature, and to present a description of the “state of the art” at low-strain amplitudes. Here we restrict ourselves mainly to the question of dynamic nonlinearity and do not take up the equally important question of the nature of loss mechanisms and their connection and interaction with the nonlinear (compliant) behavior underlying the frequency shift.

[7] In the past, several different groups have carried out resonant bar experiments. *Gordon and Davis* [1968] investigated a large suite of crystalline rocks, including Quartzite, Granite, and Olivine basalt, at strains between $10^{-9} < \epsilon < 10^{-3}$. Their main objective was to measure the loss factor Q^{-1} (or the internal friction ϕ in their terminology) as a function of strain and the ratio of stress and strain. In order to cover the large strain range they divided their experiments in two components: for $10^{-9} < \epsilon < 10^{-5}$ they used the driven frequency method, driving the rocks at very high frequencies, and for $10^{-5} < \epsilon < 10^{-3}$ they made direct measurements of the stress-strain curve. Their main findings were the following.

[8] 1. The loss factor is quite insensitive to the strain amplitude, diverging from a constant value only at high strains. At these high strains they conclude that this increase in Q^{-1} is the result of internal damage.

[9] 2. Q^{-1} is highly structure sensitive; that is, it is sensitive to the details of the microstructure of the rock.

[10] 3. Q^{-1} increases as the temperature increases. They conclude that this increase is due to grain-interface displacement, and therefore alteration of the internal structure of the rock.

[11] 4. At large strains they find static hysteresis with end-point memory.

[12] Following up on *Gordon and Davis* [1968], *McKavanagh and Stacey* [1974] and *Brennan and Stacey* [1977] performed another set of stress-strain loop measurements on granite, basalt, sandstone, and concrete.

Their main objective was the measurement of stress-strain loops below strain amplitudes of $\epsilon = 10^{-5}$, since *Gordon and Davis* [1968] had reported that Q^{-1} above this limit was no longer a linear function of the applied strain. *McKavanagh and Stacey* [1974] were able to go down to strains of 10^{-6} . (Note that this level is still above the strain at which we found nonequilibrium effects to be important, *TenCate et al.* [2004].) At these strains they found that the hysteresis loops for sandstone were always cusped at the ends. Another interesting result was that below a certain strain amplitude the shape of the loop became independent of the applied strain amplitude. From this they concluded that even at the very smallest strain amplitudes, cusps should continue to be present in stress-strain loops. (However, *Brennan and Stacey* [1977] noted that for granite and basalt, the stress-strain loops do become elliptical for strains lower than 10^{-6} .) In view of our recent results [*TenCate et al.*, 2004] this conclusion might have been drawn without having enough evidence at low enough strain amplitudes. We return to this point in section 4.4.

[13] *Winkler et al.* [1979] conducted experiments with Massilon and Berea sandstone at strain amplitudes between 10^{-8} and 10^{-6} . The main goal was to determine the strains at which seismic energy losses caused by grain boundary friction become important but the change of the resonance frequency with strain amplitude was also investigated. They concluded that the frictional losses are only important at strains larger than were investigated. Additionally, they found that the two sandstones investigated displayed nonlinear features dependent on several external parameters, such as water content or confining pressure. They find that the loss factor is independent of strain below strains of 5×10^{-7} , while at relative large strain ($>10^{-6}$), there is a clear increase, in agreement with *Gordon and Davis* [1968]. The main drawback of the experiments by *Winkler et al.* [1979] is the relative lack of data points, especially in the very low strain regime; the quality of the repeatability of their measurements on the same sample is also not shown. In this respect, our work significantly improves on previous results; we increase the number of measurement points in the low-strain regime by a factor of five in comparison to *Winkler et al.* [1979], allowing a more robust analysis of the data.

[14] More recently, *Guyet et al.* [1999] and *Smith and TenCate* [2000] analyzed a set of resonant bar experiments with Berea sandstone samples also at low strains. The conclusions they reached, however, strongly disagreed with the older results of, e.g., *Winkler et al.* [1979]. Instead of the expected quadratic behavior of the frequency shift with drive at very low strains, an essential prediction of Landau theory, they reported an ostensibly linear dependence, which held down to the smallest strains. We note that such a linear decrease in several material samples was also reported by *Johnson and Rasolofosaon* [1996, and references therein], albeit at significantly higher strains.

[15] This surprising behavior was claimed to be consistent with predictions of a phenomenological model originally developed to explain (static) hysteretic behavior in geomaterials at very high strains (the Preisach-Mayergoyz space (PM space) model). In this model a rock sample is described in terms of an ensemble of mesoscale hysteretic units [*McCall and Guyet*, 1994; *Guyet et al.*, 1997]. By

applying the PM space model to low-strain regimes, a linear dependence of the frequency shift with drive can be obtained. By its very nature, the model also predicts the existence of cusps in low-amplitude stress-strain loops. As discussed in section 4.4, however, we do not detect cusps in stress-strain loops at low strains.

[16] Motivated partly by these very different findings on similar sandstones and with similar experimental setups, we embarked on a set of well-characterized resonant-bar experiments using Fontainebleau and Berea sandstone samples *TenCate et al.* [2004]. Broadly speaking, our findings for the resonance frequency shift confirm the original results of *Winkler et al.* [1979]; below a certain strain threshold ϵ_M both sandstones displayed the expected quadratic behavior. In addition, we were able to show that previous claims of a linear shift at high strains are actually an artifact due to the material conditioning mentioned above at strains higher than ϵ_M , and that a simple macroscopic Duffing model provides an excellent mathematical description of the experimental data without going beyond Landau theory (as PM space models explicitly do, by adding nonanalytic terms to the internal energy expansion). Thus we established that, to the extent macroreversibility holds, the predictions of classical theory are in fact correct.

[17] In this paper we extend our previous analysis by adding an investigation of energy loss (via the resonator quality factor Q), dynamical stress-strain loops, and harmonic generation. We carry out the same experiment several times with the same sample to demonstrate environmental control and repeatability. The data analysis is based on a Gaussian process model to avoid biasing from nonoptimal fitting procedures applied to experimental data. The Duffing model introduced in our previous work is shown to be nicely consistent with the newer results. The predictions of this model for the quality factor, the frequency shift, and hysteresis cusps (null prediction) all hold within experimental error at strains below ϵ_M . At higher strains, this simple model breaks down, as it must, due to (deliberate) exclusion of nonequilibrium effects. Finally, we have reanalyzed a subset of the data which were taken in 1999 [*Smith and TenCate*, 2000] and had led to very different conclusions for Berea samples. We show that the old experimental data are actually in good agreement with our present findings [this paper; *TenCate et al.*, 2004].

[18] The paper is organized as follows. First, in section 2 we describe the experimental setup in some detail. Next, in section 3 we explain how we analyze the data, especially how we determine the peaks of the resonance curves and how our procedure allows us to determine realistic error bars. In section 4 we discuss the results from the experiments. A simple theoretical model that describes the experimental results is presented in section 5. We compare previous findings in very similar experiments with our new results in section 6 and conclude in section 7.

2. Experiments

[19] The samples used in the experiments are thin cores of Fontainebleau and Berea sandstone (sources are Fontainebleau from IFP and Berea from Cleveland Quartz Ohio), 2.5 cm in diameter and 35 cm long. As established by X-ray diffraction measurements, Fontainebleau sandstone is

almost pure quartz (>99% with trace amounts of other materials); Berea sandstone is less pure having only $85 \pm 8\%$ quartz with $8 \pm 1\%$ feldspar and $5 \pm 1\%$ kaolinite and approximately 2% other constituents. Fontainebleau sandstone has grain sizes of around 150μ and a porosity of $\sim 24\%$. Berea sandstone samples have grain sizes which are somewhat smaller, $\sim 100 \mu$, with a porosity of about 20%.

[20] A small Bruel&Kjr (B&K) 4374 accelerometer is carefully bonded to one end of each core sample with a cyanoacrylate glue (SuperGlue gel, Duro). The accelerometers are an industry standard, well characterized, and calibrated. With perfect bonding between accelerometer and rock, the accelerometer, and the associated B&K 2635 Charge Amp, has a flat frequency and phase response to 25 kHz. With poor bonds, the upper frequency limit of the flat response drops. Thus great care is taken to establish a good bond between accelerometer and sample. Each accelerometer is first qualitatively tested (i.e., finger pressure) to be sure of a strong bond. Furthermore, before samples are placed in the environmental isolation chamber (discussed below) for measurements, a comparison of the accelerometer response with a laser vibrometer (Polytec) is made and accelerometers are rebonded if the frequency responses differed noticeably. In any case, it is important to point out that for the samples used in this study, all of the resonance frequencies are below 3 kHz, nearly an order of magnitude below the upper frequency flat response limit for the accelerometer/charge amp combination.

[21] The source excitation is provided by a 0.75 cm thick piezoelectric disk epoxied (Stycast 1266) to the other end of the sample core and backed with an epoxied high impedance backload (brass) to ensure that most of the acoustic energy couples into the rock sample instead of the surrounding environment. Resonances in the backload (>50 kHz) are much higher than the frequencies and resonances of the sample and thus are not excited in our experiments.

[22] For all the experiments described here, the lowest-order longitudinal mode (first Pochhammer mode) is excited. (We note that the mass of the brass backload lowers the center frequencies of the Pochhammer mode resonances somewhat but does not affect the shape of a resonance curve.) Resonance curves are easy to measure and analyze and fairly high strains can be attained without requiring a high-power amplifier (with its frequently accompanying nonlinearities). For Fontainebleau sandstone the lowest resonance frequency is around 1.1 kHz; for Berea sandstone the lowest resonance frequency is around 2.8 kHz. Measured values for the quality factor Q of these resonances are about 130 for the Fontainebleau sandstone sample and about 65 for the Berea sandstone sample. The lowest-order Pochhammer mode has both compressional and shear components but the motion is nevertheless quasi-one-dimensional and the bulk of the sample participates in the wave motion associated with the resonance. As higher-order Pochhammer modes begin to resemble surface waves, only the very lowest frequency modes are examined here.

[23] Samples are suspended at two points with loops of synthetic fiber (dental floss) or thin O rings. Different

suspension points slightly alter the lowest Pochhammer mode resonance frequencies but these differences are much smaller than differences caused by even slight changes of temperature; moreover, and perhaps more importantly, once the bar is mounted, the resonance frequencies do not change with increasing drive levels when tested with a standard (an acrylic bar). Suspended in this way (stress-free ends) the sample's lowest Pochhammer resonance frequency corresponds to roughly a half wavelength in the sample.

[24] Since most rocks are extremely sensitive to temperature and temperature changes [*Ide*, 1937], with relaxation times of several hours, we have built a sample chamber for effective environmental isolation. A second inner 3/4-inch-wall Plexiglas box with caulked seams holds both the samples which are suspended from the top of the box. Air-tight electrical feedthroughs are available for driver and accelerometer connections. The entire chamber is flushed with N_2 gas and then placed inside another (larger) Plexiglas box and surrounded with fiberglass insulation and sealed. The inner sample chamber also sits on top of gel pads for vibration isolation. The complete isolation chamber is placed in a room whose temperature is controlled with a thermostat and typically varies by no more than $3^\circ C$ over the course of an entire daily temperature cycle and less than a degree over the course of a single experiment. Measured resonance frequencies of samples in this box have been stable to within 0.1 Hz.

[25] To get the most precise measurements possible, we use an HP 3325B Frequency synthesizer with a crystal oven for frequency stability as the signal source. The signal from the HP 3325B is fed into the reference input of an EG&G 5301A Lock-In amplifier which compares that reference signal with the measured signal from the accelerometer via a B&K 2635 charge amplifier. The whole experiment, including data acquisition, is computer controlled via LabVIEW and a GPIB bus. To drive the source, the signal from the HP frequency synthesizer is fed into a Crown Studio Reference I amplifier and matched to the (purely capacitive) piezoelectric transducer via a carefully constructed and tested linear matching transformer.

[26] To test all the electronics for linearity, we have constructed several known linear sample standards of nearly identical geometry to the rock samples. The density, sound speed, and Q 's of the samples are chosen such that the mechanical impedances $\rho \times c$ are similar to those of the rock samples. These "standard" samples are driven with identical source/backloads and at levels similar to those experienced by the rock samples. No nonlinearities have been seen; results for an acrylic rod are shown in Figure 1.

[27] With the present isolation system, we have verified long-term frequency stability of the samples to ± 0.1 Hz (corresponding to a long-term thermal stability inside the chamber of 10 mK), which is close to how well the peak of the frequency response curve can be determined at the lowest levels of strain shown in this paper. To test the sensitivity of the Lock-In amplifier and assembled apparatus, we have measured a resonance curve on the Fontainebleau sample at an extremely low drive level. The result is shown in Figure 2. The acceleration measured by the accelerometer has been converted to strain (the open circles) using the driving frequency f via $\epsilon = \ddot{u}/(4\pi L f^2)$

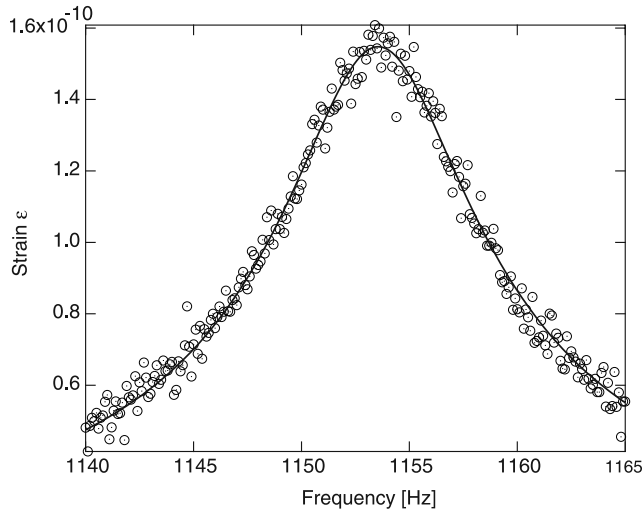


Figure 2. Low-amplitude drive resonance curve for Fontainebleau sandstone. The solid curve is a Lorentzian fit to the data points.

following the convention by *TenCate et al.* [2004], where L is the length of the bar and \ddot{u} is the acceleration. Even though the peak strain near the resonance frequency is only about 1.6×10^{-10} , the shape of the resonance curve is clear with only minimal noise obscuration: a Lorentzian curve is an extremely good fit to the data as shown by the solid line. (Error bars are not shown for clarity.) With computer control and long-term temperature stability due to the isolation chamber, this experimental setup permits long enough times to take data over a large, and an order of magnitude lower, range of strains not studied previously.

3. Data Analysis

[28] The basic quantities measured in a resonance experiment are frequency f and calibrated accelerometer voltage V , which is automatically converted into acceleration \ddot{u} . It is convenient to translate the acceleration to a strain variable in order to make the comparison of different samples with different lengths easier. As stated in section 2, we employ the convention $\epsilon = \ddot{u}/(4\pi Lf^2)$. These measurements lead to resonance curves as shown, e.g., in Figure 1. The task now is to determine the peaks of the resonance curves, tracking the shift of the resonance frequency as a function of the strain as displayed in Figure 3.

[29] In this paper we use a statistical analysis based on a nonparametric Gaussian process to model the strain ϵ as a function of the driving frequency f . The flexibility of the Gaussian process model for strain allows for estimation of the resonance frequency and resulting strain (f^* , ϵ^*) without assuming a parametric form for the dependence of strain on driving frequency. Drawbacks of using a parametric model can include understated uncertainties regarding resonance quantities (f^* , ϵ^*) and excessive sensitivity to measurements far away from the actual resonance frequency. The nonparametric modeling approach avoids both of these possible pitfalls.

[30] For a given experiment, observations (f_i, ϵ_i) , $i = 1, \dots, n$ are taken. The observed strain is modeled as a smooth function of frequency plus white noise δ :

$$\epsilon_i = z(f_i) + \delta_i, \quad i = 1, \dots, n, \quad (1)$$

where the smooth function $z(f)$ is modeled as a Gaussian process and each δ_i is modeled as an independent $N(0, \sigma^2)$ deviate. The Gaussian process model for $z(f)$ is assumed to have an unknown constant mean μ and a covariance function of the form

$$C[z(f_i), z(f_j)] = \sigma_z^2 \rho^{-|f_i - f_j|^2}. \quad (2)$$

The model specification is completed by specifying prior distributions for the unknown parameters σ^2 , μ , σ_z^2 , and ρ . After shifting and scaling the data so that the f_i 's are between 0 and 1, and the ϵ_i 's have mean 0 and variance 1, we fix μ to be 0 and assign uniform priors over the positive real line to σ^{-2} and σ_z^{-2} , and a uniform prior over $[0, 1]$ to ρ .

[31] The resulting analysis gives a posterior distribution for the unknown function $z(f)$ which we take to be the resonance curve. This posterior distribution quantifies the updated uncertainty about $z(f)$ given the experimental observations. We use a Markov chain Monte Carlo (MCMC) approach to sample realizations from the posterior distribution of $z(f)$ over a dense grid of points in the neighborhood of the resonance frequency f^* [Banerjee et al., 2004]. From each of these MCMC realizations of $z(f)$ the resonance frequency f^* and the corresponding maximum strain $\epsilon^* = z(f^*)$ are recorded. This creates a posterior sample of pairs (f^*, ϵ^*) which are given by the dots in Figure 4a. Figures 4b and 4c show the posterior uncertainty for f^* and ϵ^* separately with histograms of these posterior samples. We use the posterior mean as point estimates for f^* and ϵ^* . In the paper we use error bars that connect the 5th

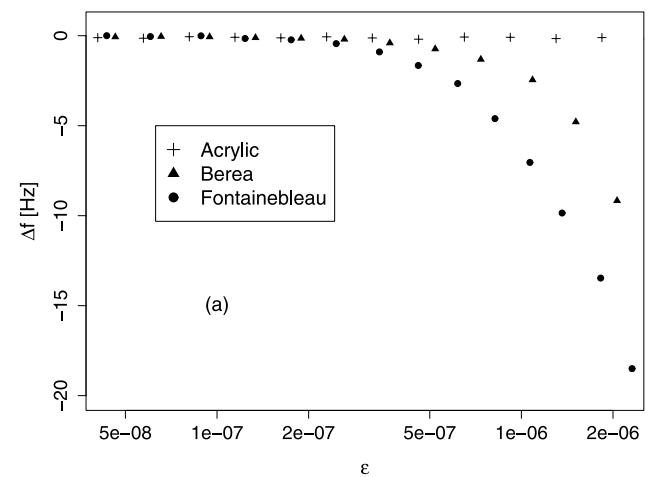


Figure 3. Resonance frequency shift Δf as a function of the effective strain ϵ for the three samples shown in Figure 1. The reference center frequencies are the same for Figure 1.

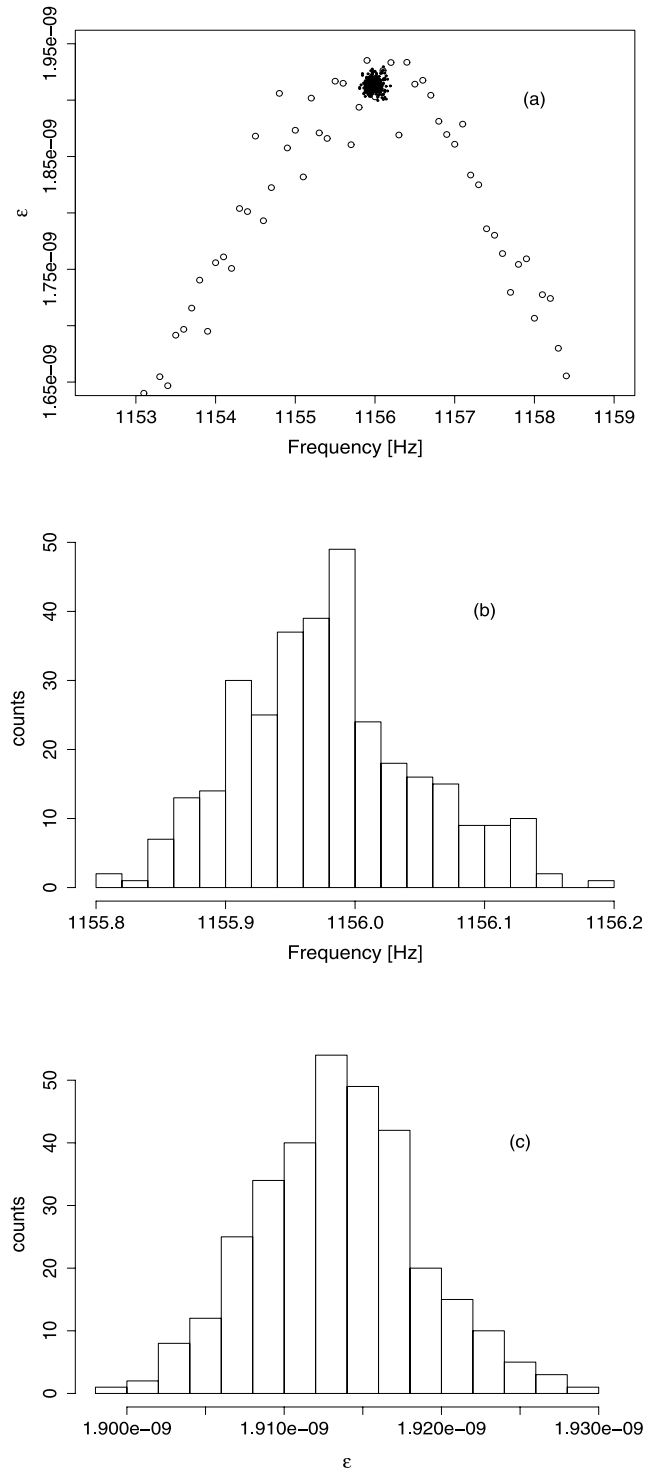


Figure 4. (a) Resonance curve for Fontainebleau at a strain $\sim 2 \times 10^{-9}$. The central cluster of dots is the MCMC posterior sample of pairs (f^*, ϵ^*) that define the resonance peak. (b) Frequency peak distribution and (c) frequency peak strain distribution from the MCMC analysis for the same resonance curve shown in Figure 4a.

and the 95th percentiles of the posterior samples to quantify the uncertainty in our estimates.

4. Experimental Results

4.1. Memory Effects and Conditioning

[32] We have recently established the existence of two strain regimes [TenCate et al., 2004]. As mentioned in section 1, in the first regime (strains below ϵ_M) the material displays a reversible decrease of the resonance frequency with strain, while in the second regime, (nonequilibrium) memory and conditioning effects become apparent. The second regime is entered at the strain threshold ϵ_M which depends on the material and the environment (e.g., temperature, saturation etc.). To determine ϵ_M for these samples, the following experiments are performed.

[33] A reference resonance curve is obtained at the lowest strain possible. The resonance frequency is determined and used as a reference frequency f_0 for the following procedure. The source excitation level is increased, a new resonance curve is obtained, and then followed immediately by dropping the excitation level back in an attempt to repeat the reference resonance curve. If there are no memory effects, the repeated curve's resonance frequency should match the initial reference frequency. If memory effects are at play, they will persist and the repeated curve's peak resonance frequency will be lower than the original. An example of this is shown in Figure 5. This procedure is repeated for incrementally increasing excitation levels until memory effects become measurable. The excitation level (and strain) where memory effects first become noticeable defines ϵ_M for that sample.

[34] The existence of the two regimes delineated by ϵ_M is crucial to understanding and interpreting the dynamical behavior of geomaterials. Although it is possible to

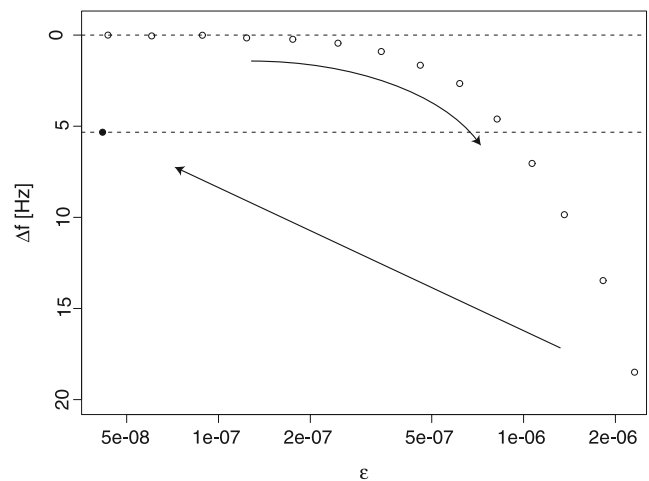


Figure 5. Example of resonance frequency shift showing the conditioning effect. The drive is increased up to a strain of 2×10^{-6} and afterward the rock is driven again at the lowest strain. The black dot shows the value of the resonance frequency peak after the last drive application. The difference between the two values for Δf at the lowest strain demonstrates the effect of conditioning. The sample used in this figure is Fontainebleau and the reference center frequency is 1155.98 Hz.

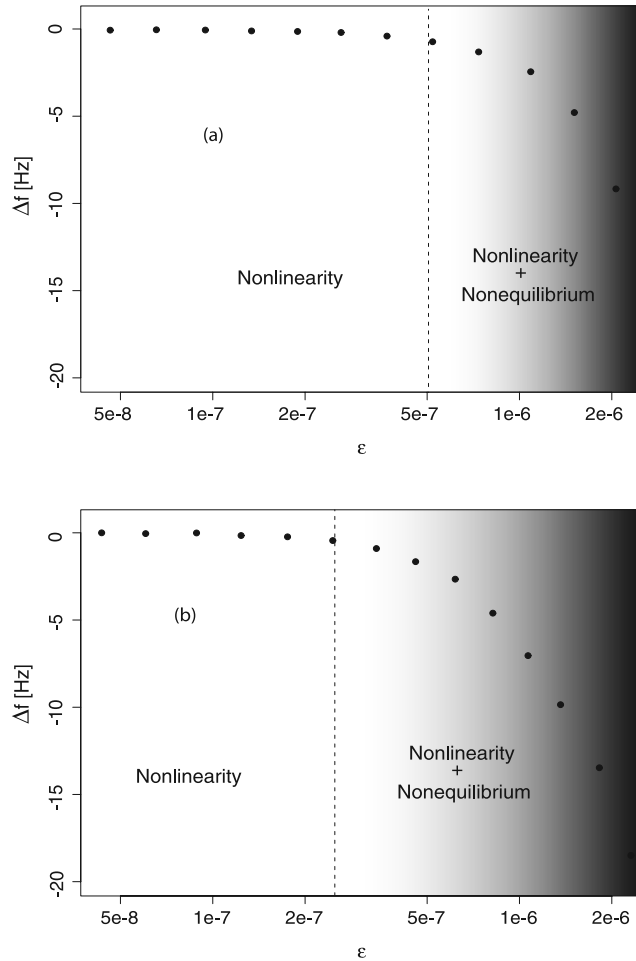


Figure 6. Resonance frequency shift versus strain. The first regime where the material displays only an intrinsic reversible nonlinearity is shown unshaded, and the second regime which combines nonlinear and nonequilibrium effects is shaded in gray. The threshold strain for (a) Berea is $\epsilon_M \simeq 5 \times 10^{-7}$ and (b) for Fontainebleau is $\epsilon_M \simeq 2 \times 10^{-7}$. Since ϵ_M is not only a material specific constant but can also depend on environmental variables, such as temperature and humidity, we show the regime in which nonlinearity and nonequilibrium are mixed, not as one solid block, but rather as a region in different shades of gray. It is important to note that the data points in the shaded regions depend on the (temporal) experimental protocol, whereas the data points in the unshaded regions characterize an invariant behavior. The reference center frequency is 2765 Hz for Berea and 1155.98 Hz for Fontainebleau.

describe the nonlinearity of the material at strains below ϵ_M with classical theory [Landau and Lifshitz, 1998], above ϵ_M the experimental results are complicated by conditioning effects due to the nonequilibrium dynamics of the rock. Disentangling the intrinsic nonlinearity of the material and these nonequilibrium effects is very difficult and the frequency shifts in dynamical experiments at strains above ϵ_M do not have a simple interpretation. In particular, classical elasticity theory assumes thermodynamic reversibility and therefore cannot be applied in this essentially nonequilibrium situation. By the same token,

classical theory cannot be tested by experiments carried out in this regime. It is clear that a new theoretical framework for the second regime, one that combines nonlinearity with nonequilibrium dynamics, is definitely needed.

[35] Figures 6a and 6b show our data for the resonance frequency shifts versus strain for Berea and Fontainebleau samples, respectively. The first regime where the material displays only the intrinsic reversible nonlinearity is shown in the unshaded area, whereas the regime which combines nonlinear and nonequilibrium dynamical effects is shaded in gray. The strain threshold for Berea is $\epsilon_M \simeq 5 \times 10^{-7}$ and 2×10^{-7} for Fontainebleau under the present experimental conditions. For the remaining part of the paper we will focus only on the intrinsic nonlinear regime which is uncontaminated by conditioning effects and allows for a simple interpretation of the experimental data.

4.2. Intrinsic Nonlinearity

[36] In this section we describe experimental results for strains below ϵ_M . In this regime, the data are free from memory and conditioning effects and the samples display a reversible decrease of the resonance frequency with strain. For this reason it is possible to speak of, and analyze, the intrinsic nonlinearity of the material. As discussed in some detail in the Introduction, the previous history of resonance measurements and the analysis of the associated results is somewhat confusing. On the one hand, there are claims that geomaterials display essentially nonclassical nonlinear elastic behavior down to very low strains (10^{-8}) [Guyer and Johnson, 1999] with no evidence for a crossover to elastic behavior. On the other hand, earlier findings [Winkler et al., 1979], albeit with generous error bars, are inconsistent with these claims.

[37] In order to investigate this issue in a systematic and controlled fashion, we carried out repeatable resonance bar experiments at strains as low as 10^{-9} following the experimental protocols discussed above; these strains are an order of magnitude lower than those previously investigated.

[38] The results for the resonance frequency shift Δf , $\Delta f = f_0 - \Omega/2\pi$, where Ω is the (linear) resonance radian frequency, as a function of the effective strain ϵ for Fontainebleau and Berea sandstone samples are shown in Figure 7. The measured strain for Fontainebleau ranges from 2×10^{-9} to $\epsilon_M \simeq 2 \times 10^{-7}$ and from 2×10^{-9} to $\epsilon_M \simeq 5 \times 10^{-7}$ for Berea. We observe a resonance frequency shift of 0.45 Hz for Fontainebleau and 0.5 Hz for Berea in the regime below ϵ_M . The error bars shown in Figure 7 are calculated using the MCMC analysis as described in section 3. The strain error bars are smaller than the symbols used in the figures. The error bars for Δf for Berea are larger than the ones for Fontainebleau because of the smaller Q for the Berea sample: the Berea resonance curves are much wider, making the peak determination more uncertain. The resonance frequency shift observed (0.45 Hz or 0.5 Hz) is less than the errors bars by Winkler et al. [1979] experiment. Being our experiment digital, they are more precise than the analog experiment of Winkler et al. [1979]. The solid lines in Figure 7 represent the prediction of a theoretical model

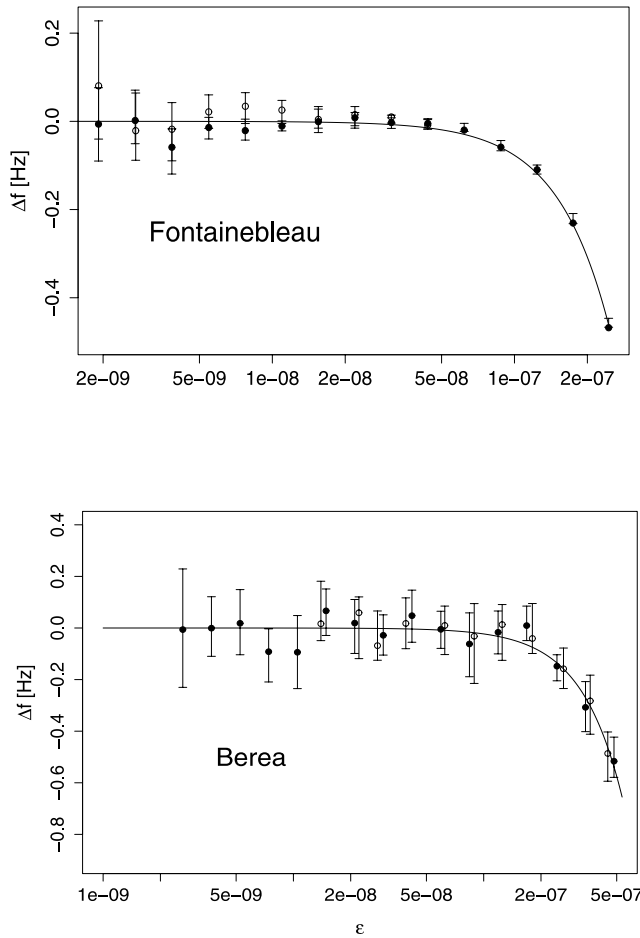


Figure 7. Resonance frequency shift Δf as a function of the effective strain ϵ for Fontainebleau and Berea samples for $\epsilon < \epsilon_M$. The reference center frequency is 2765 Hz for Berea and 1155.98 Hz for Fontainebleau. The solid lines represent predictions of a theoretical model incorporating a Duffing nonlinearity (equation (23)). Two different sets of data points obtained from the same samples are shown to demonstrate the robustness of the measurements. Note the logarithmic scale on the x axis.

with a Duffing nonlinearity described in detail in section 5.

[39] We find that the resonance frequency softens quadratically with increasing drive amplitude until the strain reaches ϵ_M , beyond which value conditioning effects also enter. This behavior can be fully described by classical nonlinear theory. At very low strains, $\sim 10^{-8}$ to 10^{-7} (lower end for Fontainebleau, upper end for Berea) the samples are effectively in a linear elastic regime. At these low strains, there is no discernible dependence of the resonance frequency on the strain, the materials behave linearly to better than 1 part in 10^4 .

4.3. Quality Factor

[40] Energy loss in solids is mostly characterized by a frequency-independent loss factor (“solid friction”) in contrast to liquid friction. Nevertheless, rocks are known to display characteristics of liquid friction as a function of pore fluid loading [e.g., *Born*, 1941] with an associated depen-

dence of the loss factor $1/Q$ (Q is also termed the quality factor) on the frequency. It appears that the unusual nature of wave attenuation in geosolids remains to be fully studied and understood [cf. *Knopoff and MacDonald*, 1958]. As pointed out by Knopoff and MacDonald, a frequency-independent Q cannot be explained by a linear theory of attenuation, however, it is unlikely that the nonlinearity should be associated with amplitude since even for very small strains, Q remains finite.

[41] In the present work we do not focus on the dependence of Q on frequency at small strains, but investigate the dependence on strain amplitude as an alternative probe of dynamical nonlinearity for effective strains $\epsilon < \epsilon_M$. We measure the Q from the amplitude resonance curves directly, using

$$Q = \frac{2\pi f_0}{\Gamma} [1 + \mathcal{O}(1/Q^2)], \quad (3)$$

where Γ is the width of the response curve measured at the points $a_0/\sqrt{2}$ where a_0 is the peak amplitude. This definition of Q is strictly valid only for linear systems but, as will be discussed further below, at low strains the amplitude response curves are effectively those of a linear system, albeit with a peak frequency shift. At leading order, the Q as defined in (3) is independent of the nature of the loss mechanism (solid or liquid friction).

[42] The loss factor thus depends on two variables, the amplitude response peak frequency and the width Γ of the response curve. We certainly expect it to change as a function of the strain simply because f_0 is a function of the strain amplitude. This is, however, a very small change, fractionally of order 10^{-4} . Aside from this expected variation, what is of more interest is whether Γ is also a function of the strain.

[43] In Figure 8a we show measurements of the variation in the relative width $\Delta\Gamma/\Gamma_0$ for the Fontainebleau sample. As mentioned in section 4.1, we restrict ourselves to the strain regime below ϵ_M to prevent contamination of the results by nonequilibrium effects. The width Γ can only be measured to an accuracy of $\sim 1\%$, the error bars being obtained from MCMC analysis of the resonance curves. To this accuracy, the results of Figure 8a demonstrate that $\Delta\Gamma/\Gamma_0$ is essentially constant (except for the single highest strain point) as is the case for linear systems. This result is also consistent with the predictions of the Duffing model discussed below in section 5.

[44] The measurement of the relative change in quality factor is shown in Figure 8b and, given the smallness of the frequency peak shift, simply reflects the behavior of $\Delta\Gamma/\Gamma_0$. We note that except for the highest strain point, our results are in agreement with a strain-independent quality factor within the displayed errors. To summarize, to the extent that we have investigated the strain dependence of acoustic losses ($\epsilon < \epsilon_M$), no unexpected behavior has been found.

4.4. Stress-Strain Loops and Harmonic Generation

[45] At very low strains and at the frequencies of interest here, one would expect the resonant bar system to be essentially a damped, driven harmonic oscillator and the hysteresis curve to be an ellipse. This is in contrast to the situation in (quasi)static hysteresis where “pointed” or

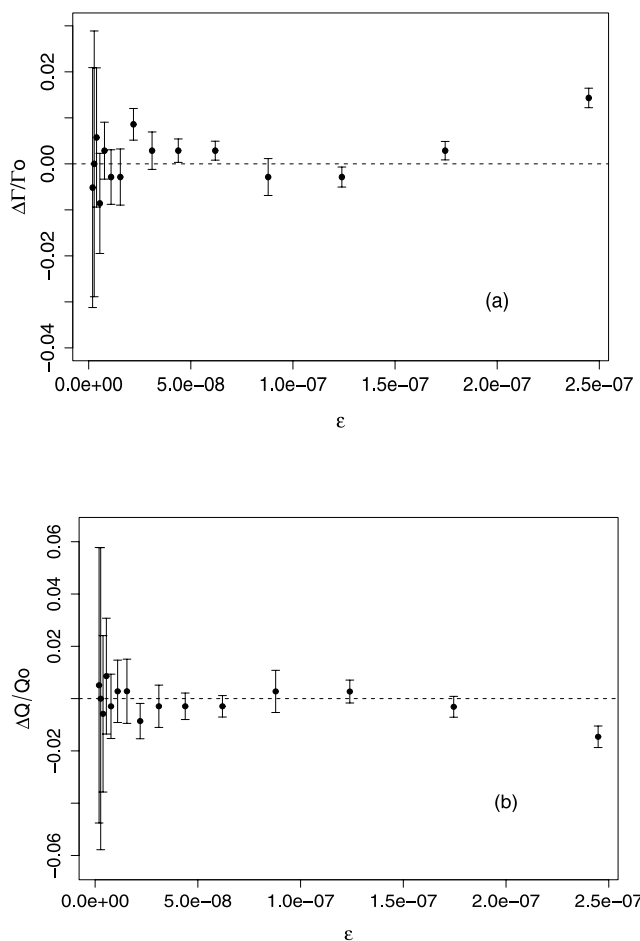


Figure 8. Fontainebleau. (a) Variation of the width Γ of the resonance curve peak. (b) Variation of the quality factor Q with strain.

“cusped” loops are observed due to sources of inelasticity that do not fit in to the simple viscoelastic model. Whether low-strain loops at some point become elliptical was investigated by *McKavanagh and Stacey* [1974, p. 250], who came to the conclusion that this was not the case at strains $\sim 10^{-5}$ for sandstone and indeed that “...cusped loops extend to indefinitely small strain amplitudes.” On the other hand, *Brennan and Stacey* [1977] found that for granite and basalt, loops became elliptical at strain values lower than 10^{-6} . These statements were made with data taken at low frequencies, less than 0.1 Hz, thus do not directly apply to our experiment unless the underlying sources of inelasticity continue to be relevant at high frequencies.

[46] Experimental evidence for cusped stress-strain loops led to the theoretical description of nonequilibrium dynamics in geomaterials via PM space models which are based on static-hysteretic building blocks. In previous work, it has been argued that these models provide a correct description of the dynamics of rock even at small strains [*McCall and Guyer*, 1994]) and at high frequencies [cf. *Guyer et al.*, 1999]. Our dynamical experiments allow us to analyze stress-strain loops at very low strains in the kHz frequency range and to detect the existence of pointed or cusped loops. As evident in Figure 9, the loops are elliptical

with no evidence for cuspy behavior. Thus we find no evidence to support the existence of “nonlinear” dissipation mechanisms, as invoked in PM space models, at kHz frequencies. Predictions of the simple Duffing model introduced by *TenCate et al.* [2004] and described in detail in section 5, are completely consistent with the data.

[47] Our experimental results are shown in Figure 9. We plot the acceleration versus the amplitude of the drive applied to the bar for both the Berea (Figure 9a) and Fontainebleau (Figure 9b) samples. In the case of Fontainebleau, the strain is 1×10^{-7} at a frequency of 1154 Hz while for Berea the strain is 2.5×10^{-7} at a frequency of 2754.5 Hz. (Note that these experiments are carried out after the original resonance curve measurements were completed. Because of different environmental factors, e.g., temperature, the resonance frequencies of the samples have shifted slightly.) Acceleration and drive amplitude are proportional to the strain and the stress, respectively. The acceleration and the drive voltage are measured as functions of time and the time series is stored once steady state was attained. In Figure 9, a piece of the time series is displayed and the

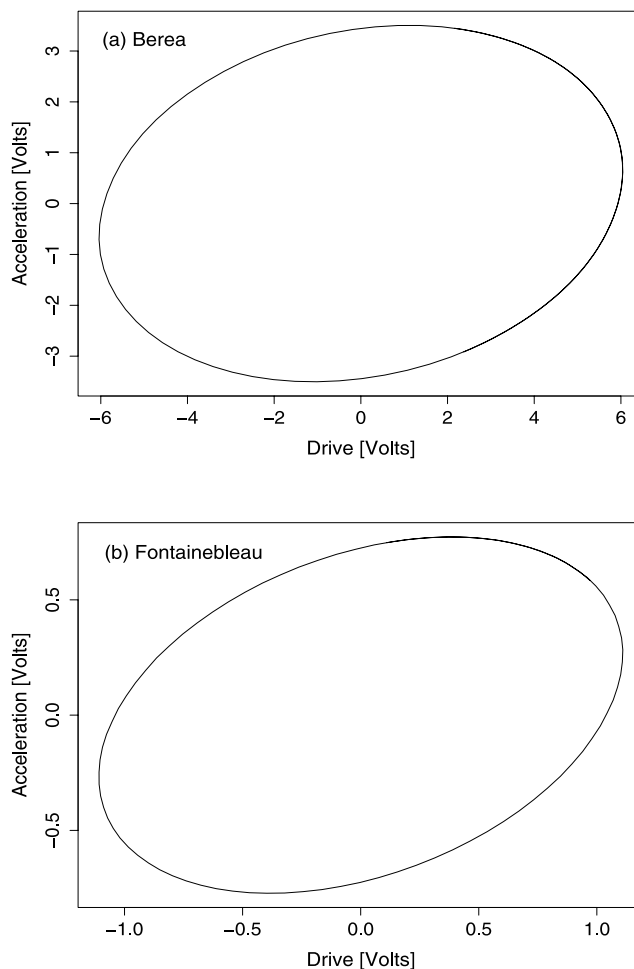


Figure 9. Acceleration versus drive amplitude for the (a) Berea and (b) Fontainebleau samples. The acceleration and the drive voltage are proportional to the strain and the stress, respectively. Berea strain amplitude is 2.5×10^{-7} at a frequency of 2754.5 Hz; Fontainebleau strain amplitude is 10^{-7} at a frequency of 1154 Hz. Note the absence of cusps.

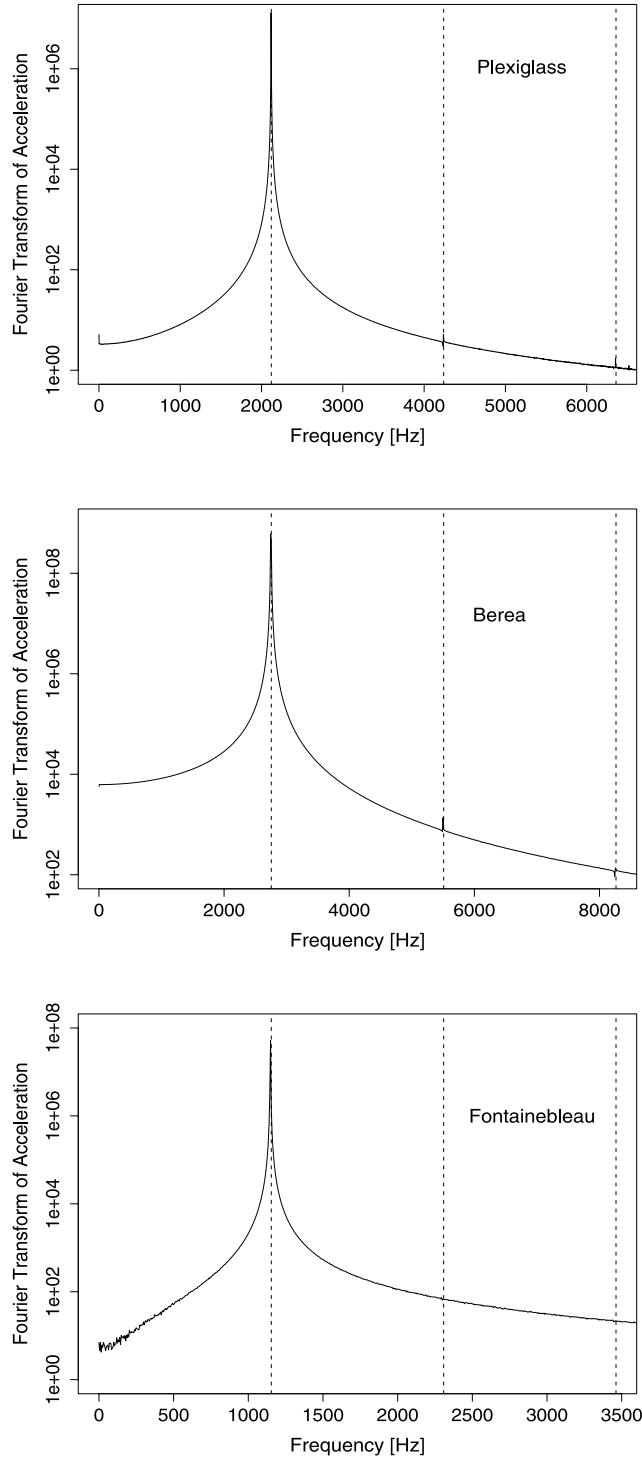


Figure 10. Fourier transform of the acceleration taken at the resonance frequency for acrylic, Berea, and Fontainebleau (semilog plot). Acrylic has a nominal strain of 2.6×10^{-6} at frequency 2120 Hz; Berea has a nominal strain of 2.5×10^{-7} at 2754.5 Hz; Fontainebleau has a nominal strain of 10^{-7} at frequency 1154 Hz. The dashed lines show the positions of the first, second, and third harmonics. Harmonic generation is not detected. The two spikes which occur in Plexiglas and Berea are due to the residual nonlinearity of the experimental apparatus.

acceleration shifted by 180° . For both samples, there is no evidence for cusps in the stress-strain loops.

[48] Another important question is whether the nonlinearity evidenced by the peak frequency shift can also be detected by searching for harmonic generation in resonant bar and wave propagation experiments. The interpretation of results from wave propagation experiments is somewhat ambiguous [Meegan *et al.*, 1993; TenCate *et al.*, 1996] due to experimental complications (e.g., reflective losses). However, harmonic detection in (potentially much cleaner) resonant bar experiments has been previously reported [cf. Johnson *et al.*, 1996]. Johnson *et al.* found substantial harmonic generation in rock samples, including Berea and Fontainebleau, at strains as low as 10^{-7} .

[49] In this paper, we present our results in a search for harmonics at strains $\epsilon < \epsilon_M$. Figure 10 shows spectral measurements for a linear material (acrylic) and the two rock samples. Dashed lines indicate where first, second, and third harmonics of the fundamental are expected to appear (these are not the higher Pochhammer modes). In all three cases we observe no evidence for the existence of higher-order harmonics. The two small spikes which occur in the data for Plexiglas (acrylic) and Berea are due to the residual nonlinearity of the experimental apparatus.

5. The Model

[50] In this section we introduce a simple phenomenological model which describes the nonlinear behavior of the rock samples under consideration. This model does not include a treatment of memory and nonequilibrium effects and is therefore not meant to apply in the regime where these effects become important, i.e., for strains greater than ϵ_M . A more complex model which applies also to the higher-strain regimes will be described elsewhere. As shown by us previously [TenCate *et al.*, 2004], a quartic (Duffing) potential nonlinearity augmenting a damped harmonic oscillator yields results that accurately describe the data in the low-strain regime. This model predicts a quadratic decrease of the resonance frequency as a function of drive amplitude, as expected from the theory of classical nonlinear elasticity.

[51] The equation of motion for the displacement is taken to be

$$\ddot{u} + \Omega^2 u + 2\mu\dot{u} + \gamma u^3 = F \sin(\omega t), \quad (4)$$

where $\gamma < 0$ leads to a softening nonlinearity as observed in the experiment (e.g., Figure 1). The driving force on the right hand side represents the drive applied to the rods in the experiment. The frequency Ω is the (unshifted) harmonic oscillator frequency (for $\gamma, \mu = 0$) and μ is the linear damping coefficient. In the following we briefly discuss a convenient analytic approximation for the solution of equation (4).

5.1. Multiscale Analysis

[52] Since the displacement u is small we can solve the equation of motion (4) analytically and predict the decrease of the frequency with the drive amplitude. We employ multiscale perturbation theory to obtain a useful closed-

form solution to equation (4). In the following we describe how this approach works and how to extract model parameters from experimental data. [For a complete derivation of multiscale perturbation theory see *Nayfeh*, 1981]. While one can of course solve equation (4) numerically, the analytic approach yields simple formulae which provide much better physical intuition.

[53] A naive approach to solving equation (4) would be a straightforward expansion of the displacement in the form

$$u(t, \alpha) = u_0(t) + \alpha u_1(t) + \dots \quad (5)$$

This ansatz is justified for small displacements. Inserting the expansion of u in the equation of motion and keeping only terms of $\mathcal{O}(\alpha)$ leads to two differential equations for u_0 and u_1 :

$$\ddot{u}_0 + \Omega^2 u_0 = F \sin(\omega t), \quad (6)$$

$$\ddot{u}_1 + \Omega^2 u_1 = -2\mu \dot{u}_0 - \gamma u_0^3, \quad (7)$$

which are simply harmonic oscillators with an inhomogeneity on the right-hand side. The equation for u_0 (6) can be solved immediately and the solution inserted into the right hand side of the equation of motion for u_1 (7) specifying the inhomogeneity for u_1 completely. The solution for u_1 can now be determined and a perturbative solution for u itself can be obtained by inserting u_0 and u_1 into equation (5). A detailed analysis of this solution for $u(t)$ leads to the following result: for specific values of ω resonances occur, the case $\omega \sim \Omega$ leading to a primary resonance causing the solution for u to diverge. To determine a solution for equation (4) free from this problem, the method of multiple scales can be used [Nayfeh, 1981]. The idea is the following: besides assuming that the displacement is small, we also assume that the nonlinearity is small. In addition we assume that the excitation, the damping, and the nonlinearity are all of the same order in α . This leads to a modified equation of motion for u :

$$\ddot{u} + \Omega^2 u + 2\alpha \mu \dot{u} + \alpha \gamma u^3 = \alpha F \sin(\omega t). \quad (8)$$

Further, we introduce two timescales, a slow scale $T_1 = \alpha t$ and a fast timescale $T_0 = t$ which leads to a transformation of the derivatives of the form

$$\frac{d}{dt} = D_0 + \alpha D_1, \quad (9)$$

$$\frac{d^2}{dt^2} = D_0^2 + 2\alpha D_0 D_1 + \dots, \quad (10)$$

with $D_i = \partial/\partial T_i$. Expanding u in the form

$$u = u_0(T_0, T_1) + \alpha u_1(T_0, T_1) \quad (11)$$

and keeping again only terms of order α leads to the following set of differential equation for u_0 and u_1 :

$$D_0^2 u_0 + \Omega^2 u_0 = 0, \quad (12)$$

$$D_0^2 u_1 + \Omega^2 u_1 = -2D_0 D_1 u_0 - 2\mu D_0 u_0 - \gamma u_0^3 + F \sin(\omega T_0). \quad (13)$$

The difference with the previous naive expansion becomes clear immediately: While earlier the driving force was part of the differential equation for u_0 , it is now part of the inhomogeneity of u_1 . A general solution for u_0 is given by

$$u_0 = A(T_1) e^{i\Omega T_0} + \bar{A}(T_1) e^{-i\Omega T_0}. \quad (14)$$

Inserting equation (14) into the differential equation for u_1 (13) yields

$$D_0^2 u_1 + \Omega^2 u_1 = - (2iA'\Omega + 2i\mu A\Omega + 3A^2 \bar{A}\gamma) e^{i\Omega T_0} - A^3 \gamma e^{3i\Omega T_0} + \frac{1}{2} F e^{i\omega T_0} + \text{c.c.} \quad (15)$$

Since we are only interested in the case $\omega \sim \Omega$, i.e., driving near to the resonance frequency we introduce a detuning parameter

$$\omega = \Omega + \alpha \sigma \Rightarrow \omega T_0 = \Omega T_0 + \sigma T_1. \quad (16)$$

Inserting (16) into the differential equation (15), expressing A in the polar form $A = 1/2a \exp i\beta$, defining a new parameter $\phi = \sigma T_1 - \Omega\beta$ and $\phi' = \sigma - \Omega\beta'$, and eliminating the secular terms from the resulting equation, we arrive at the following solution for $u(t)$:

$$u = a \cos(\omega t - \phi) + \mathcal{O}(\alpha), \quad (17)$$

$$a' = -a\mu + \frac{1}{2} \frac{F}{\Omega} \sin \phi, \quad (18)$$

$$a\phi' = a\sigma - \frac{3}{8} \frac{\gamma a^3}{\Omega} + \frac{1}{2} \frac{F}{\Omega} \cos \phi. \quad (19)$$

After a sufficiently long time, a and ϕ will reach a steady state hence their derivatives will vanish and the left hand sides of equations (18) and (19) will be zero. Squaring the equations and adding them leads to the so-called frequency response equation

$$\Omega^2 \mu^2 a^2 + a^2 \left(\sigma \Omega - \frac{3}{8} a^2 \gamma \right)^2 = \frac{1}{4} F^2. \quad (20)$$

Equation (20) can be solved with respect to σ

$$\sigma = \frac{3}{8} a^2 \frac{\gamma}{\Omega} \pm \frac{1}{2a\Omega} \sqrt{F^2 - 4\mu^2 a^2 \Omega^2}. \quad (21)$$

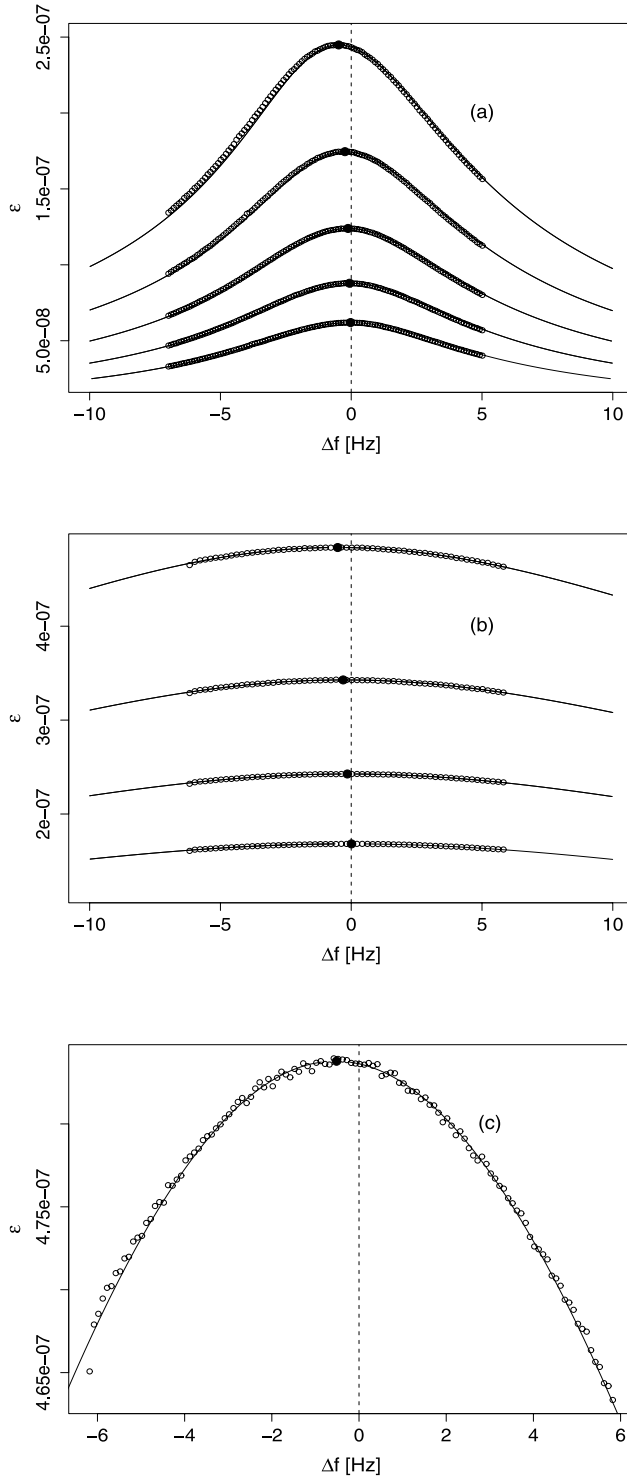


Figure 11. Average strain amplitude ϵ as a function of drive frequency for (a) Fontainebleau and (b) and (c) Berea. The reference center frequency is 1155.98 Hz for Fontainebleau and 2765.179 Hz for Berea. The open circles are the experimental data; the solid circles mark the peak positions. The solid lines are theoretical predictions from equation (20). Figure 11c shows in detail the resonance curve at the highest strain for Berea.

As σ has to be real, the maximum value for a (which we label a_0) and therefore the peak of the response curve can be immediately determined:

$$F^2 = 4\mu^2 a_0^2 \Omega_0^2 \Rightarrow a_0 = \frac{F}{2\mu\Omega}, \quad (22)$$

and therefore

$$\sigma_0 = \frac{3F^2\gamma}{32\mu^2\Omega^3}. \quad (23)$$

Thus the model predicts a quadratic decrease of the frequency with the drive amplitude F . The model also predicts the invariance of the resonance curve width Γ for any strain. Solving equation (20) for σ and substituting $a = a_0/\sqrt{2}$ we obtain

$$\Gamma = 2\mu. \quad (24)$$

Note that the approximation ignores corrections of $\mathcal{O}(1/Q^2)$. These are numerically small on the scale of the experimental errors. At this leading order of the approximation, the effect of the nonlinearity is simply to produce an effective harmonic oscillator response, with a frequency shift and peak height dependent on the drive amplitude.

5.2. Constraints on the Model Parameters From the Experimental Data

[54] The Duffing model predicts an invariant resonance curve width Γ , therefore we first measure this quantity from the experimental resonance curves. Consistent with the above expectation, we find that Γ is constant within 1% for both samples over the applicable strain range; using relation (24), we then immediately determine the damping coefficients $\mu = 27.5 \text{ s}^{-1}$ for the Fontainebleau and $\mu = 131.6 \text{ s}^{-1}$ Berea sample, respectively. Using the definition of $\sigma_0 = 2\pi f_0 - \Omega$ and the relation $F = 2\mu\Omega L\epsilon/\pi$ we can rewrite equation (23) in terms of the effective strain ϵ and the resonance frequency f_0 as

$$f_0 = \frac{3L^2\gamma}{16\pi^3\Omega} \epsilon^2 + \frac{\Omega}{2\pi}. \quad (25)$$

The linear resonance frequency Ω and the nonlinearity parameter γ now follow by fitting the experimental data for f_0 as a function of the effective strain using the previous equation. We obtain the following values: the nonlinearity parameter, $\gamma = -7.6 \times 10^{19} \text{ m}^{-2} \text{ s}^{-2}$ for the Fontainebleau sample, and $\gamma = -5.3 \times 10^{19} \text{ m}^{-2} \text{ s}^{-2}$ for the Berea sample, whereas the corresponding linear resonance frequencies are 7262.8 rad/s and 17375.7 rad/s.

5.3. Comparison of Experimental Results With the Model

[55] After determining model parameters as above, we compare the Duffing model predictions with the experimental results described in section 4.

[56] We begin by investigating the predictions for the resonance curves themselves, as given in equation (20). In Figure 11 we show the results from the experiments as circles and the results from the Duffing model as solid lines

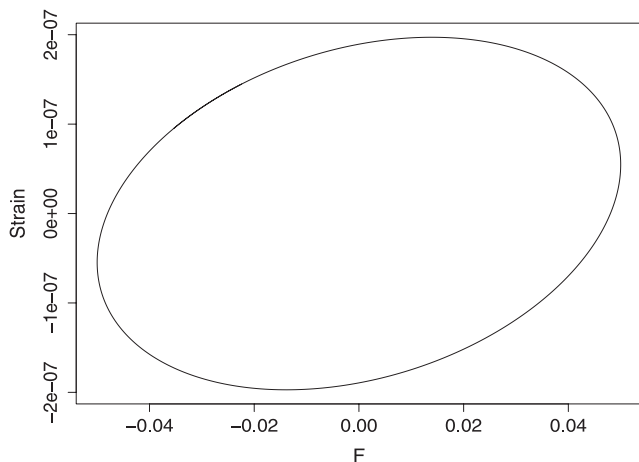


Figure 12. Hysteresis loop as predicted by the Duffing model using Berea parameters, strain 2.7×10^{-7} , frequency = 2765.3 Hz.

for Fontainebleau (Figure 11a) and Berea (Figure 11b), where Figure 11c shows a single Berea resonance curve on a smaller range in Δf to demonstrate more clearly how well the model works. In addition, it was shown earlier (Figure 7) how the resonance frequency shifts as a function of strain for Fontainebleau and Berea from both the experiment and the model. Figures 7 and 11 clearly demonstrate the excellent agreement between the experimental data and the model predictions.

[57] In Figure 12 we show the stress-strain loop obtained from the Duffing model: no cusps are present in agreement with the experimental results. Moreover our model indicates that the response of the bar to the external drive is dominated by the fundamental mode and there is no excitation due to mode-coupling of any higher harmonics as shown in Figure 13. Our model predictions are again in very good agreement with the experimental results.

6. Comparison With Previous Results

[58] As already discussed in section 1, experiments similar to the one described in this paper have been carried out in the past with somewhat confusing results. Some of them, e.g., those of *Winkler et al.* [1979], are in qualitative agreement with our findings though with less control over errors, while other papers claim quite different results. Among this second set of papers, two papers are experimentally very close to the present work (two of the authors of the current paper were involved in these experiments): the papers by *Guyer et al.* [1999] (hereinafter referred to as GTJ) and *Smith and TenCate* [2000] (hereinafter referred to as ST). We now address the question why such differing conclusions were arrived at earlier. In order to provide the answer we reanalyze a subset of the older data sets investigated in GTJ and ST (the GTJ data set is a small subset of the ST data).

[59] The sample under consideration was a Berea sandstone rod of similar size used in this paper. In order to reduce effects from moisture contained in the sandstone the sample was kept under vacuum for an extended period. This

increased the quality factor to $Q = 300$ which is roughly five times higher than in the current one, where $Q = 65$. (In GTJ the quality factor is quoted to be $Q = 170$, the discrepancy arising due to measuring Q from the width of the resonance curve at half maximum of the amplitude rather than at $1/\sqrt{2}$ of the maximum.) The resonance frequency in the old experiment was $f \sim 2880$ Hz, which is close the resonance frequency of the sample we investigated, $f \sim 2755$ Hz. In the old experiments, different measurements were made at different temperatures.

[60] Unlike our experiments, these experiments were carried out in three different strain ranges at different times: at very low strain, at medium strain, and at high strain. The main result found by GTJ was a linear fall-off of the resonance frequency peak with increasing strain while ST concluded from the same experimental data that the resonance frequency peak fell off first linearly and then quadratically with increasing strain.

[61] We first investigate a subset of the old data set in exactly the same way as in the new experiments. The results are shown in Figure 14. Figure 14a shows three sets of resonance curves at different strain ranges. The peaks of the resonance curves are determined with our MCMC analysis method as described in section 3 and marked by the solid circles. In Figure 14b the peaks of the resonance curves are plotted versus the strain. The solid lines in the low- and medium-strain regime represent the predictions from our model. In these two regimes the predictions from the Duffing model are excellent, and no unexpected behavior, such as a linear fall-off is observed. The measurements in the high-strain regime are contaminated by nonequilibrium effects and therefore our simple model is not applicable.

[62] After verifying that the old experimental data in no way contradict the results from our new experiments we now turn to the analysis strategies used in GTJ and ST and the interpretations of their findings.

[63] The results for the dependence of the resonance frequency versus strain are shown in Figure 3a in GTJ. The three different curves GTJ show are from different measurements and in all cases the dynamic range is very

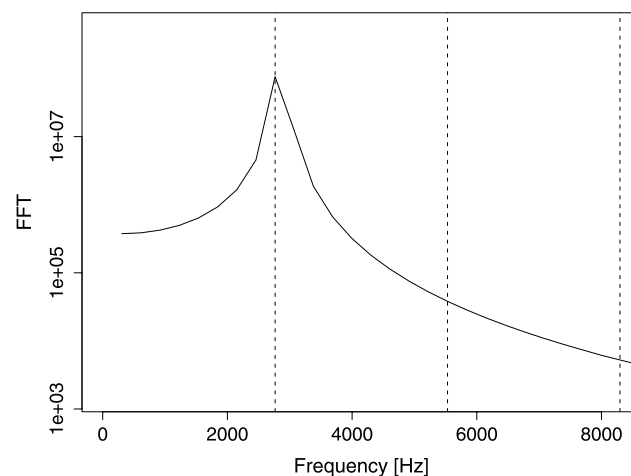


Figure 13. Spectral response from the Duffing model using Berea parameters, strain 2.7×10^{-7} , frequency = 2765.3 Hz.

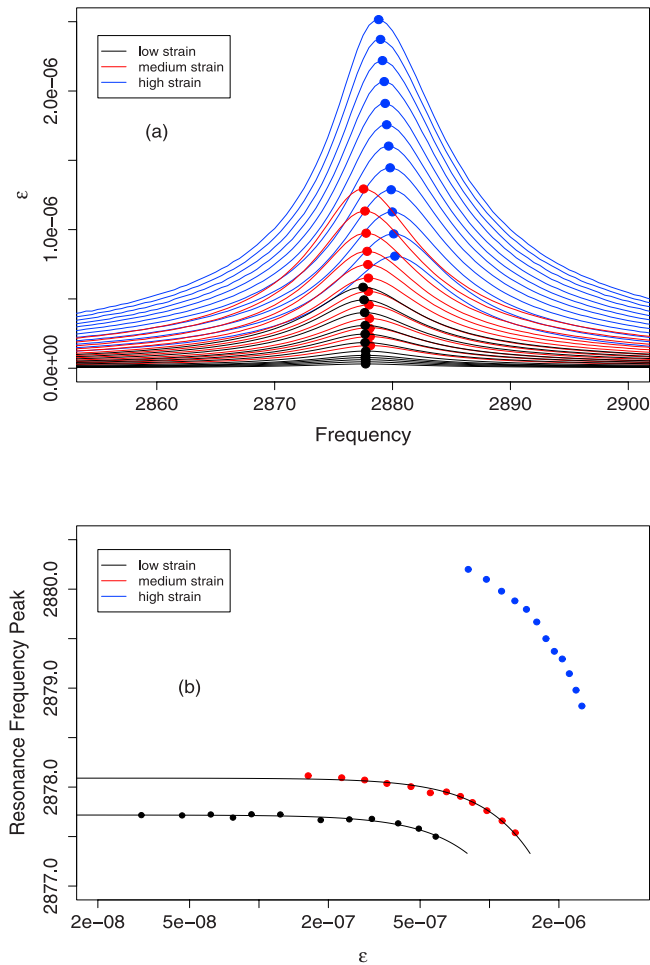


Figure 14. Comparison with previous experiments on Berea. (a) Resonance frequency curves for three sets of experiments at three different strain ranges. (b) Corresponding resonance frequency peaks. Note the logarithmic scale on the x axis. The solid lines represent predictions of the theoretical model (see equation (23)).

small. Consider now the lowest, and longest, of these curves, the strain range here is only 10^{-7} to 3×10^{-7} .

[64] To emphasize the importance of having sufficient dynamic range, we return to Figure 14b and consider only the lowest-strain measurement data set, shown in detail in Figure 15. The dashed line marks the strain corresponding to the lowest strain in GTJ in their longest strain range measurement. We show in red the best linear fit to all the data points on the right of this line. The highest strain in GTJ was 3×10^{-7} so would only include 4 of the data points in Figure 15. If we only concentrate on the strain regime to the right of the dashed line, both fits, linear and quadratic are acceptable. However, if we consider all the available data points down to the lowest strain, the linear fit fails by being too high. Therefore, in order to make a definite statement about the best fit to the data it is clearly important to have a sufficient range in strain. To summarize: the experimental data in GTJ is apparently correct, but the dynamic range of the data points analyzed is not sufficient

to draw any conclusion regarding the nonlinear behavior of the material.

[65] Next, we turn to the results found in ST. One of the main objectives in that work was to investigate the dependence of the frequency shift (hence the shift in the Young's modulus) as a function of temperature changes. Experiments at temperatures ranging from 35° to 65° were carried out. In addition different strain regimes were investigated at different times, as shown in the previous Figure 14a. The condition of the rock might have changed in between these different times, which could have led to a contamination of the results. For each temperature, the three different sets of measurements at different strains shifted in order to obtain a single measurement over a wide strain range. This approach is likely to lead to a bias in the result since the rock might have been in different metastable conditioned states for each data set.

[66] In the final step, the relative shift in the Young's modulus was determined and fitted by a single function for all resonance frequency shift curves, independent of the temperature at which they were taken or the resonance frequency f_0 (recall the different strain ranges of the data in Figure 14). The result of this analysis is shown in Figure 6 of ST. It is immediately clear that a single fit to all the curves does not work particularly well. The functional form of the fit, first linear and then quadratic, is therefore also not very meaningful any other functional form, such as pure quadratic, would have probably worked as well.

[67] The authors' contention that the temperature insensitivity of the coefficients determining the frequency shift is directly related to the underlying loss mechanism, and hence rules out thermal activation mechanisms, cannot be justified. The relationship between the frequency shift and the loss mechanism is yet to be elucidated: As shown in the present work, for example, nonlinear frequency shifts and linear losses can easily coexist, and it is well known that the loss factor is temperature-dependent.

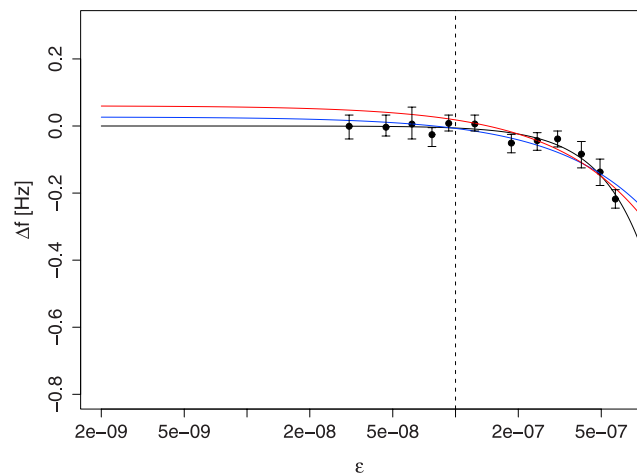


Figure 15. Comparison of different fits for the old Berea data set. Note the logarithmic scale on the x axis. The black line shows the quadratic fit obtained from the Duffing model; the red line shows the best linear fit including data points only to the right of the dashed line. The reference center frequency is 2877.78 Hz.

[68] In summary, the measurements used in GTJ and ST are in fact in very good agreement with our current measurements and understanding of the nonlinearities in rocks below a certain strain threshold: It is the interpretation of the data in these two papers that must be corrected. In GTJ the strain range over which the analysis was carried out was insufficient to reach any conclusive result about the fall-off of the resonance frequency peak with strain. In ST the fitting procedure applied to the data sets seems to have led to erroneous conclusions about the behavior of Δf versus strain.

7. Summary and Outlook

[69] In this paper we have described a set of resonant bar experiments carried out for Berea, Fontainebleau, and acrylic (as a linear control material) in order to investigate the dynamic compliance and loss mechanisms at low strains, between 5×10^{-8} and 2×10^{-6} . To ensure isolation from environmental influences, such as temperature and humidity, an isolation chamber was employed to obtain controlled and repeatable results.

[70] The main conclusion of our work is the demarcation of two strain regimes: in the first regime the material displays reversible decrease of the resonance frequency, while in the second regime, which occurs after a material and environment-dependent threshold ϵ_M , nonequilibrium and conditioning effects become important. Some of these results were previously reported in a short communication [TenCate et al., 2004]. Here we report the results of a detailed study for the first strain regime, below ϵ_M , for both Berea and Fontainebleau samples measuring quantities such as the quality factor, stress-strain loops, and amplitudes of higher harmonics. By repeating measurements on the same samples we have demonstrated the robustness of the results. At strains characteristic of reversible nonlinear behavior, the quality factor is essentially constant, but it is possible that it reduces at higher strain values. It is not unreasonable to speculate that unlike the resonance frequency shift, the amplitude dependence of the quality factor is connected to the onset of nonequilibrium behavior, but this aspect requires further investigation.

[71] The data analysis was carried out using a statistical method based on a Gaussian process model. This parameter-free method avoids any biasing of the analysis due to fitting of the resonance curves with specific functional forms. It also determines reliable error bars for the resonance frequency shift Δf as a function of the applied drive strength. The vast majority of previous papers analyzing similar experiments do not provide a detailed error analysis.

[72] A theoretical framework for the experimental results is provided by a simple damped Duffing model for which closed-form results can be obtained. The Duffing model predictions are in excellent agreement with the entire set of experimental measurements over the strain regime $\epsilon < \epsilon_M$.

[73] While in this paper, we have focused on the reversible nonlinear regime ($\epsilon < \epsilon_M$), future work will target the understanding of the nonequilibrium behavior of geomaterials. The investigation of this second regime is at the same time fascinating and very challenging. It is difficult, but essential, to disentangle conditioning/nonequilibrium and nonlinear effects. New experimental strategies have to be

developed for this endeavor. At the same time a theoretical framework which encompasses and explains all known physical effects needs to be developed.

[74] **Acknowledgments.** This work was funded in part through the DOE Office of Basic Energy Science and the Institute of Geophysics and Planetary Physics of Los Alamos National Laboratory (IGPP).

References

- Banerjee, S., B. P. Carlin, and A. E. Gelfand (2004), *Hierarchical Modeling and Analysis for Spatial Data*, CRC Press, Boca Raton, Fla.
- Born, W. T. (1941), The attenuation constant of Earth materials, *Geophysics*, *6*, 132–148.
- Bourbie, T., O. Coussy, and B. Zinszner (1987), *Acoustic of Porous Media*, Gulf, Houston, Tex.
- Brennan, B. J., and F. D. Stacey (1977), Frequency dependence of elasticity of rock—Test of seismic velocity dispersion, *Nature*, *268*, 220–222.
- Carmichael, R. S. (Ed.) (1984), *CRC Handbook of Physical Properties of Rocks*, CRC Press, Boca Raton, Fla.
- Clark, S. P. (Ed.) (1966), *Handbook of Physical Constants*, Geophys. Soc. of Am., New York.
- Gordon, R. B., and L. A. Davis (1968), Velocity and attenuation of seismic waves in imperfectly elastic rocks, *J. Geophys. Res.*, *73*, 3917–3935.
- Guyer, R. A., and P. A. Johnson (1999), Nonlinear mesoscopic elasticity, evidence for a new class of materials, *Phys. Today*, *52*, 30–35.
- Guyer, R. A., K. R. McCall, G. N. Boitnott, L. B. Hilbert Jr., and T. J. Plona (1997), Quantitative implementation of Preisach-Mayergoyz space to find static and dynamic elastic moduli in rock, *J. Geophys. Res.*, *102*, 5281–5293.
- Guyer, R. A., J. TenCate, and P. A. Johnson (1999), Hysteresis and the dynamic elasticity of consolidated granular materials, *Phys. Rev. Lett.*, *82*, 3280–3283.
- Ide, J. M. (1937), The velocity of sound in rocks and glasses as a function of temperature, *J. Geol.*, *45*, 689–716.
- Jaeger, J. C., and N. G. W. Cook (1979), *Fundamentals of Rock Mechanics*, CRC Press, Boca Raton, Fla.
- Johnson, P. A., and P. N. J. Rasolofosaon (1996), Manifestation of nonlinear elasticity in rock: Convincing evidence over large frequency and strain intervals from laboratory studies, *Nonlin. Processes Geophys.*, *3*, 77–88.
- Johnson, P. A., B. Zinszner, and P. N. J. Rasolofosaon (1996), Resonance and elastic nonlinear phenomena in rock, *J. Geophys. Res.*, *101*, 11,553–11,564.
- Knopoff, L., and G. J. F. MacDonald (1958), Attenuation of small amplitude stress waves in solids, *Rev. Mod. Phys.*, *30*, 1178–1192.
- Landau, L. D., and E. M. Lifshitz (1998), *Theory of Elasticity*, Elsevier, New York.
- McCall, K. R., and R. A. Guyer (1994), Equation of state and wave propagation in hysteretic nonlinear elastic materials, *J. Geophys. Res.*, *99*, 23,887–23,897.
- McKavanagh, B., and F. D. Stacey (1974), Mechanical hysteresis in rocks at low strain amplitudes and seismic frequencies, *Phys. Earth Planet. Inter.*, *8*, 246–250.
- Meegan, G. D., P. A. Johnson, R. A. Guyer, and K. R. McCall (1993), Observations of nonlinear elastic wave behavior in sandstone, *J. Acoust. Soc. Am.*, *94*, 3387–3391.
- Nayfeh, A. H. (1981), *Introduction to Perturbation Techniques*, John Wiley, Hoboken, N. J.
- O'Hara, S. G. (1985), Influence of pressure, temperature, and pore fluid on the frequency-dependent attenuation of elastic waves in Berea sandstone, *Phys. Rev. A*, *32*, 472–488.
- Ostrovsky, L. A., and P. A. Johnson (2001), Dynamic nonlinear elasticity in geomaterials, *Riv. Nuovo Cimento*, *24*, 1–46.
- Sheriff, R. E. (1973) *Encyclopedic Dictionary of Exploration Geophysics*, Soc. of Explor. Geophys., Tulsa, Okla.
- Smith, E., and J. TenCate (2000), Sensitive determination of the nonlinear properties of Berea sandstone at low strains, *Geophys. Res. Lett.*, *27*, 1985–1988.
- TenCate, J. A., K. E. A. Van den Abeele, T. J. Shankland, and P. A. Johnson (1996), Laboratory study of linear and nonlinear elastic pulse propagation in sandstone, *J. Acoust. Soc. Am.*, *100*, 1383–1391.
- TenCate, J. A., D. Pasqualini, S. Habib, K. Heitmann, D. Higdon, and P. A. Johnson (2004), Nonlinear and nonequilibrium dynamics in geomaterials, *Phys. Rev. Lett.*, *93*, doi:10.1103/PhysRevLett.93.065501.
- Van Den Abeele, K. E.-A., J. Carmeliet, P. A. Johnson, and B. Zinszner (2002), Influence of water saturation on the nonlinear elastic mesoscopic response in Earth materials and the implications to the mechanism of nonlinearity, *J. Geophys. Res.*, *107*(B6), 2121, doi:10.1029/2001JB000368.

Winkler, K., A. Nur, and M. Gladwin (1979), Friction and seismic attenuation in rocks, *Nature*, 277, 528–531.

Zinszner, B., P. A. Johnson, and P. N. J. Rasolofosaon (1997), Influence of change in physical state on elastic nonlinear response in rock: Significance of effective pressure and water saturation, *J. Geophys. Res.*, 102, 8105–8120.

S. Habib, T-8, University of California, Los Alamos National Laboratory, Los Alamos, NM 87545, USA.

K. Heitmann, ISR-1, MS D466, ISR Division, Los Alamos National Laboratory, Los Alamos, NM 87545, USA.

D. Higdon, D-1, University of California, Los Alamos National Laboratory, Los Alamos, NM 87545, USA.

P. A. Johnson and J. A. TenCate, EES-11, University of California, Los Alamos National Laboratory, Los Alamos, NM 87545, USA.

D. Pasqualini, EES-9, University of California, Los Alamos National Laboratory, P.O. Box 1663, MS D443, Los Alamos, NM 87545, USA. (dondy@lanl.gov)